Electronic Supplementary Material (ESI) for Journal of Materials Chemistry A.

Electronic Supplementary Information

Crystallographic orientation – surface energy – wetting property relationships of rare earth oxides

Jason Tam,[a] Bin Feng,[b] Yuichi Ikuhara, [b] Hiromichi Ohta, *[c] and Uwe Erb*[a]

[a.] *Department of Materials Science and Engineering, University of Toronto, 184 College Street, Toronto, Ontario M5S 3E4, Canada.*

[b] *Institute of Engineering Innovation, School of Engineering, The University of Tokyo, 2-11-16 Yayoi, Bunkyo-ku, Tokyo 113-8656, Japan*

[c.] *Research Institute for Electronic Science, Hokkaido University, N20W10, Kita, Sapporo 001-0020, Japan*

*email: hiromichi.ohta@es.hokudai.ac.jp, uwe.erb@utoronto.ca

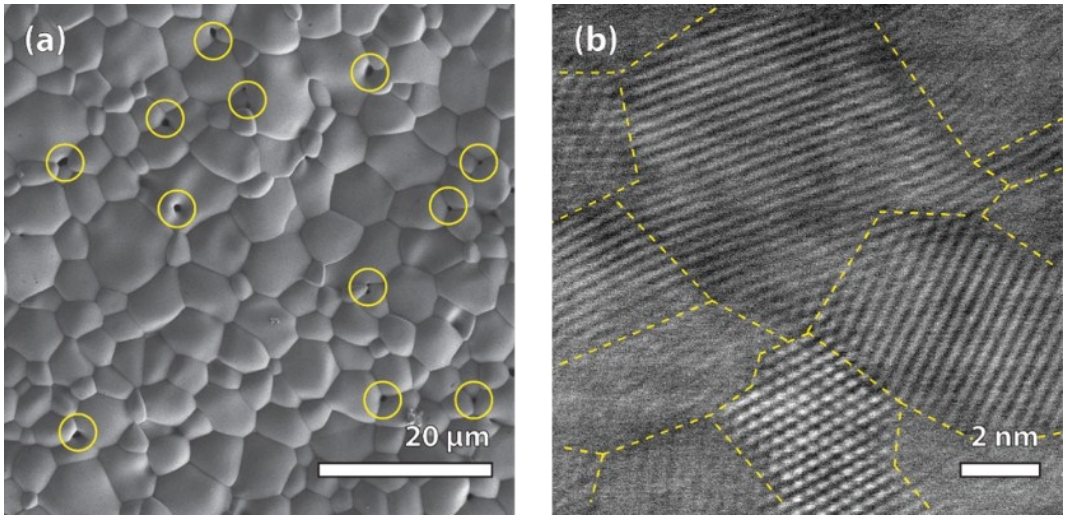

Fig. S1| (a) SEM image of a sintered CeO_2 pellet. Considerable amounts of surface roughness and porosity (circled) are present in the material. (b) HAADF-STEM image of a sputter deposited CeO_2 thin film with large fraction of high energy grain boundaries and triple junctions (outlined by the dotted lines).

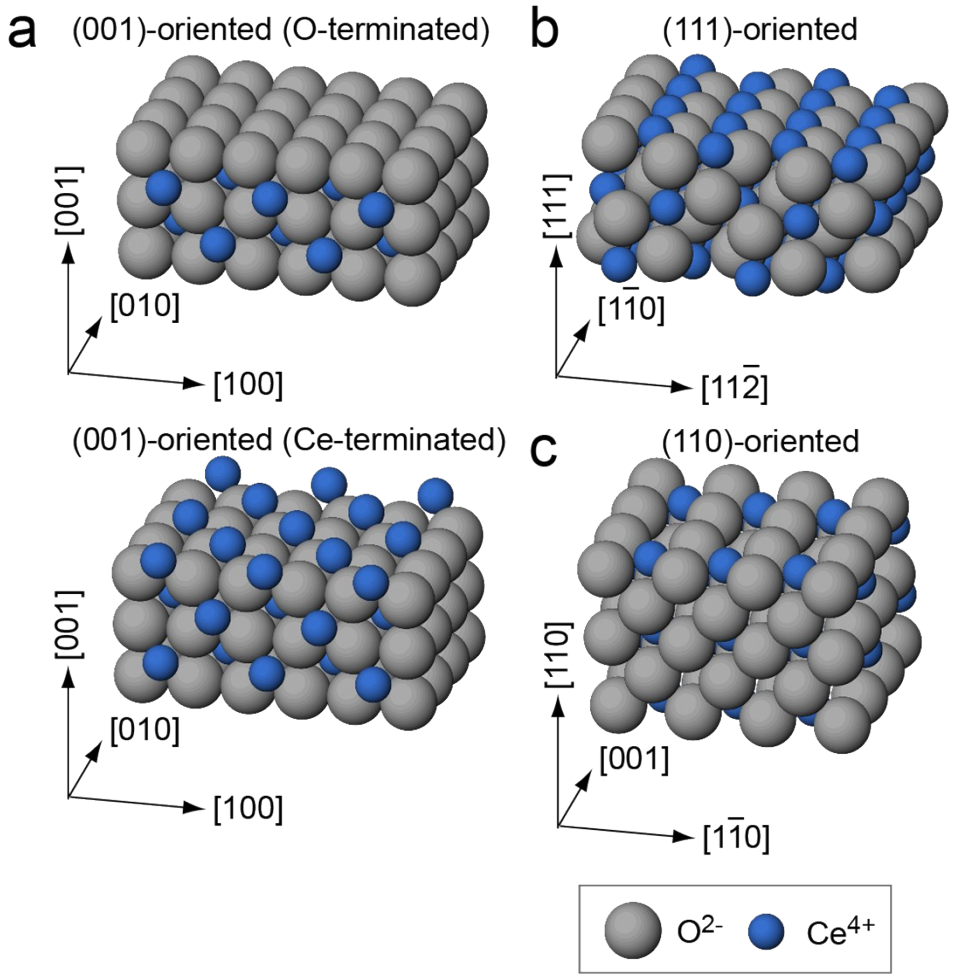

Fig. S2| Space filling models of the 3 low index orientations of CeO_2. (a) (001) orientation with alternating layers of oxygen anions and cerium cations. The surface can be O or Ce surface termination with a surface dipole moment (Tasker Type III surface, negative or positive surface charge[1]). (b) (111) orientation with close packed planes of repeating O, Ce, and O ions. There is no surface charge or dipole moment as charge neutrality is maintained for every O-Ce-O plane (Tasker Type II surface[1]). (c) (110) orientation where the composition and the charges of the Ce cations and O anions in each plane are balanced with no surface charge (Tasker Type I surface[1]).

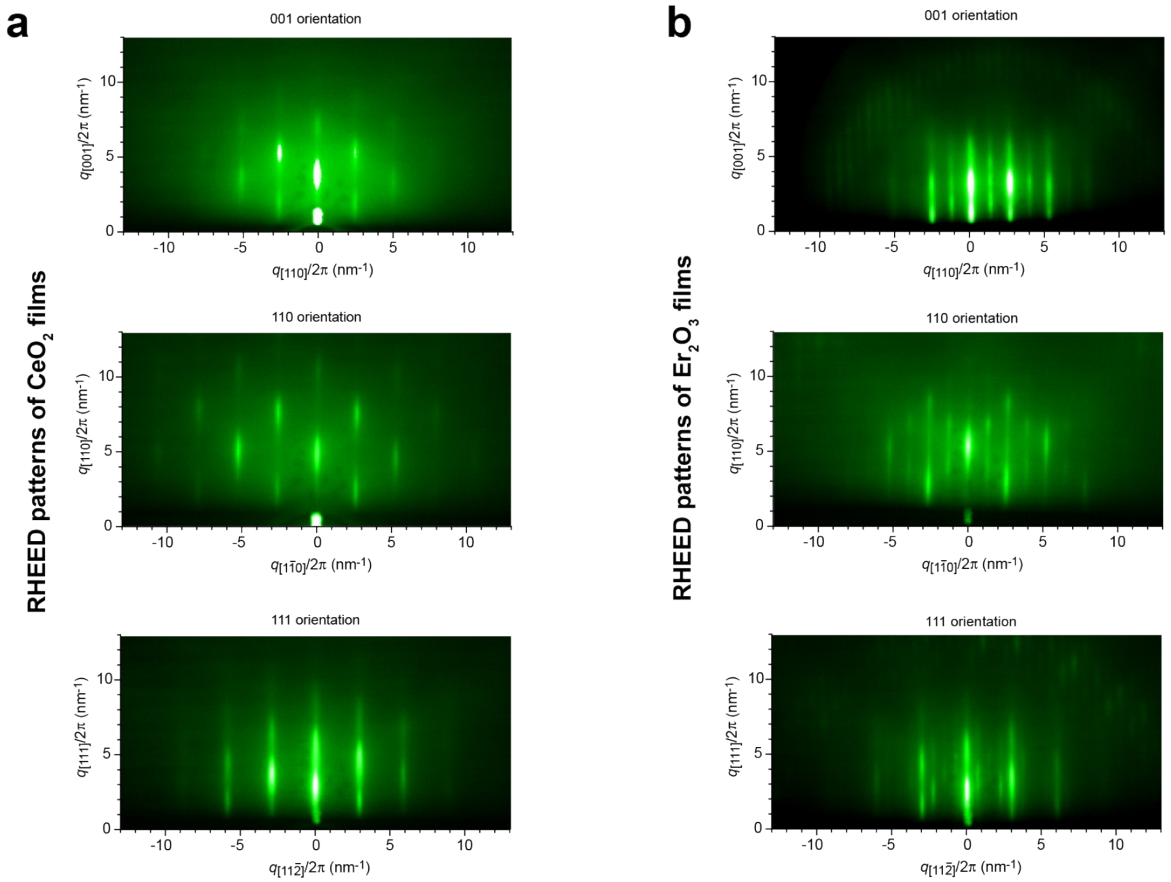

Fig. S3| RHEED patterns of (a) CeO_2 and (b) Er_2O_3 epitaxial films. Intense streaks indicate good epitaxial film growth and smoothness of the surfaces. Weak streaks observed on the Er_2O_3 RHEED patterns originated from the Er_2O_3 film (bixbyite structure), which has a different crystal structure from the YSZ substrate (fluorite structure).

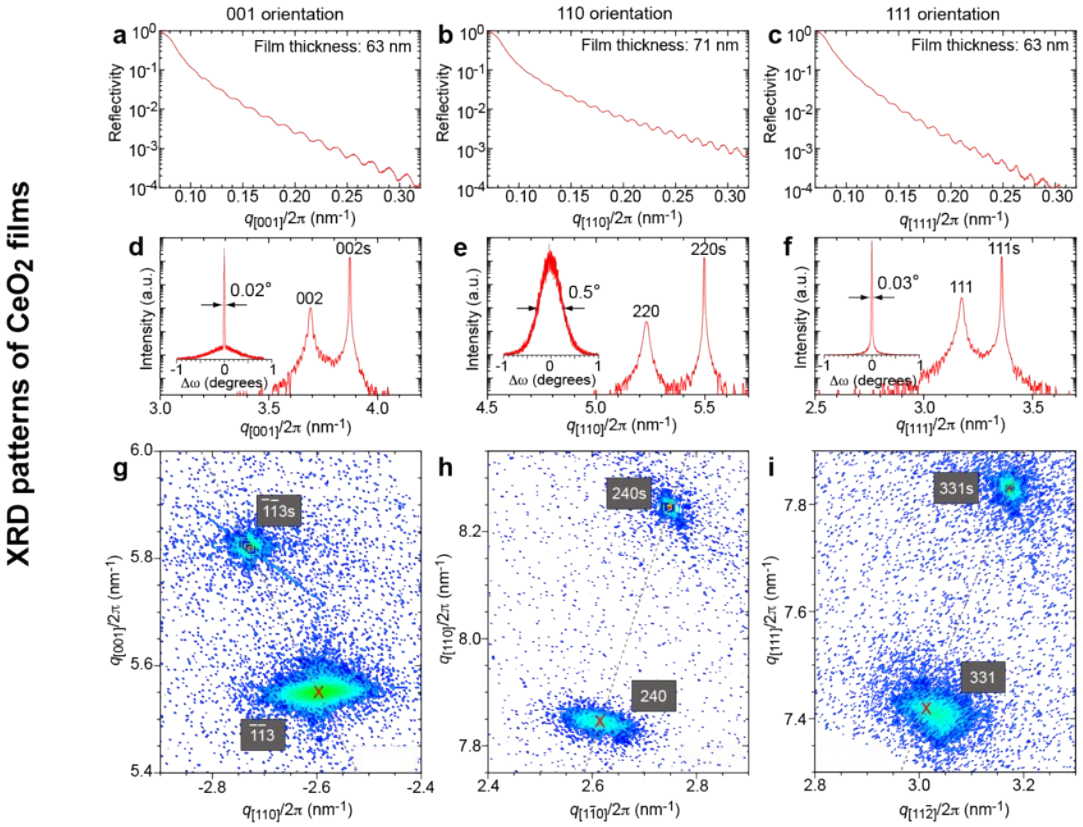

Fig. S4| X-ray characterization of CeO_2 thin films grown on YSZ substrates. (a-c) XRR curves, the Kiëssig fringes were used to calculate film thicknesses (63 – 71 nm). (d-f) Out-of-plane XRD patterns and rocking curves of the film (insets). The peaks associated with the YSZ substrates are suffixed with "s". The low (0.02 – 0.5°) full width half maximum (FWHM) of the rocking curves indicate excellent film quality. (g-i) Reciprocal space mapping around (113), (240), and (331) diffraction spots for 001, 110 and 111 oriented CeO_2 films. The red "x" symbols are the positions of the bulk CeO_2. The in-plane lattice parameter of the film was different from the substrate; The CeO_2 films were incoherently grown on the substrate, most likely due to the large lattice mismatch between the film and the substrate (+5.3 %). Moreover, the observed diffraction spots are well-matched with the bulk position in all cases, indicating that the CeO_2 crystals are fully relaxed.

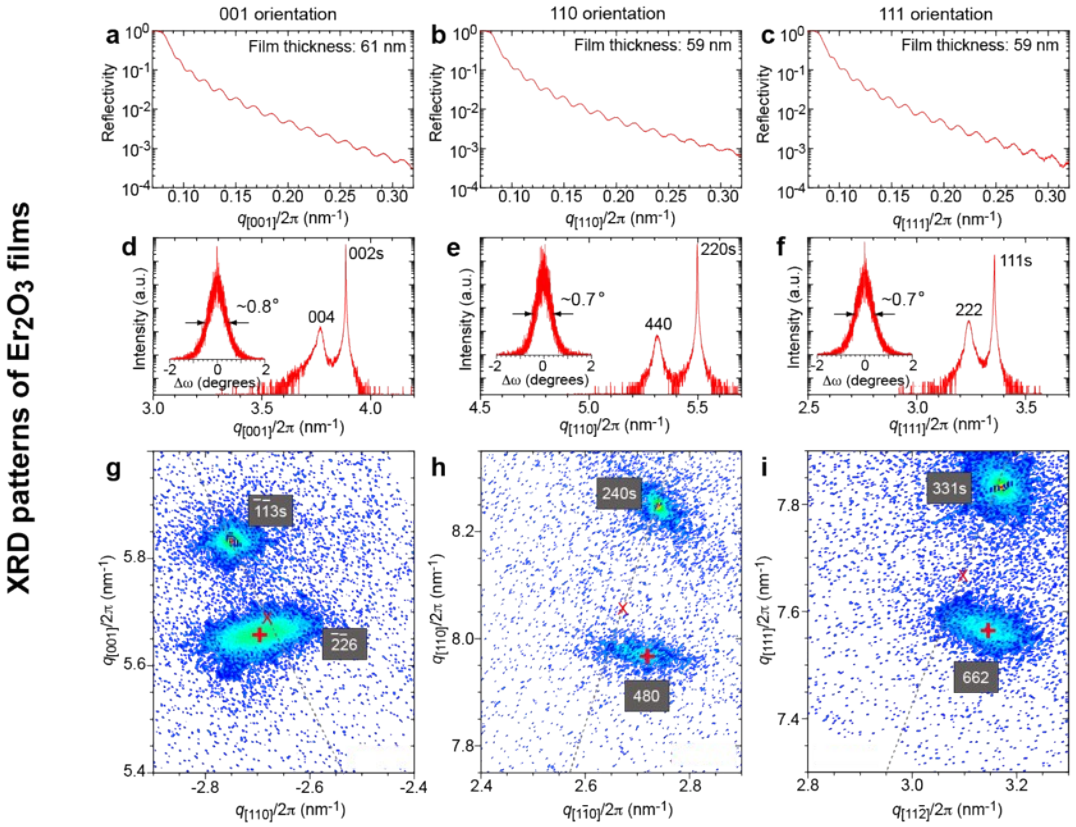

Fig. S5| X-ray characterization of Er_2O_3 thin films grown on YSZ substrates. (a–c) X-ray reflectivity (XRR) curves, the Kiëssig fringes were used to calculate film thicknesses (59 – 61 nm). (d–f) Out-of-plane XRD patterns and rocking curves of the film (insets). The peaks associated with the YSZ substrates are suffixed with "s". (g–i) Reciprocal space mapping around 226, 480, and 662 diffraction spots for (001), (110) and (111) oriented Er_2O_3 films. The red "x" symbols are the positions of the bulk Er_2O_3. The discrepancy between the intense diffraction spot of the Er_2O_3 (marked with +) and the position of the bulk Er_2O_3 (marked with x) is attributed to lattice strain caused by the lattice mismatch between the substrate and the film, as well as greater degree of crystallite tilting compared to CeO_2 films. The latter can also be seen in higher full width half maximum values in the out-of-plane rocking curve peak widths (d-f insets).

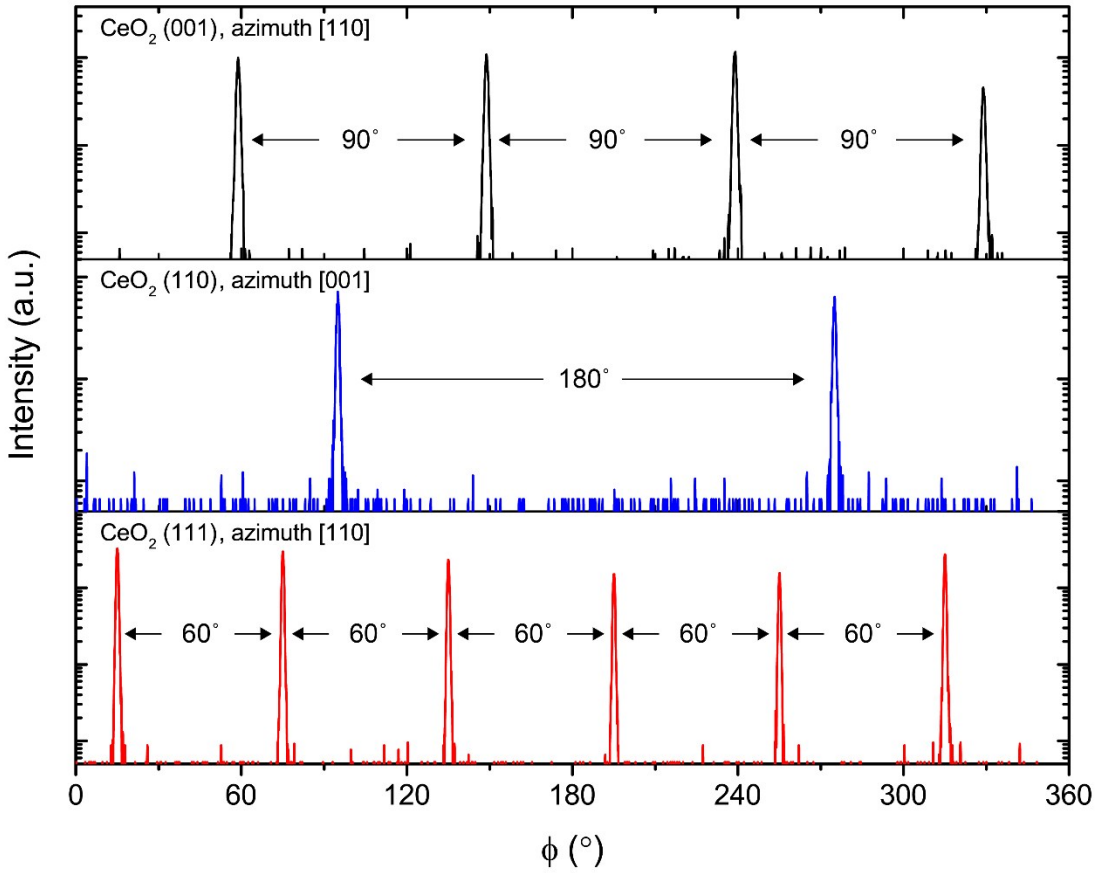

Fig. S6| In-plane rocking curves of CeO_2 films deposited onto (001), (110), and (111) YSZ substrates. The in-plane rocking curves of CeO_2 revealed that cube-on-cube epitaxial relationship with the underlying YSZ single crystal substrate, i.e. $[uvw]_{CeO_2} \,||\, [uvw]_{YSZ}$.

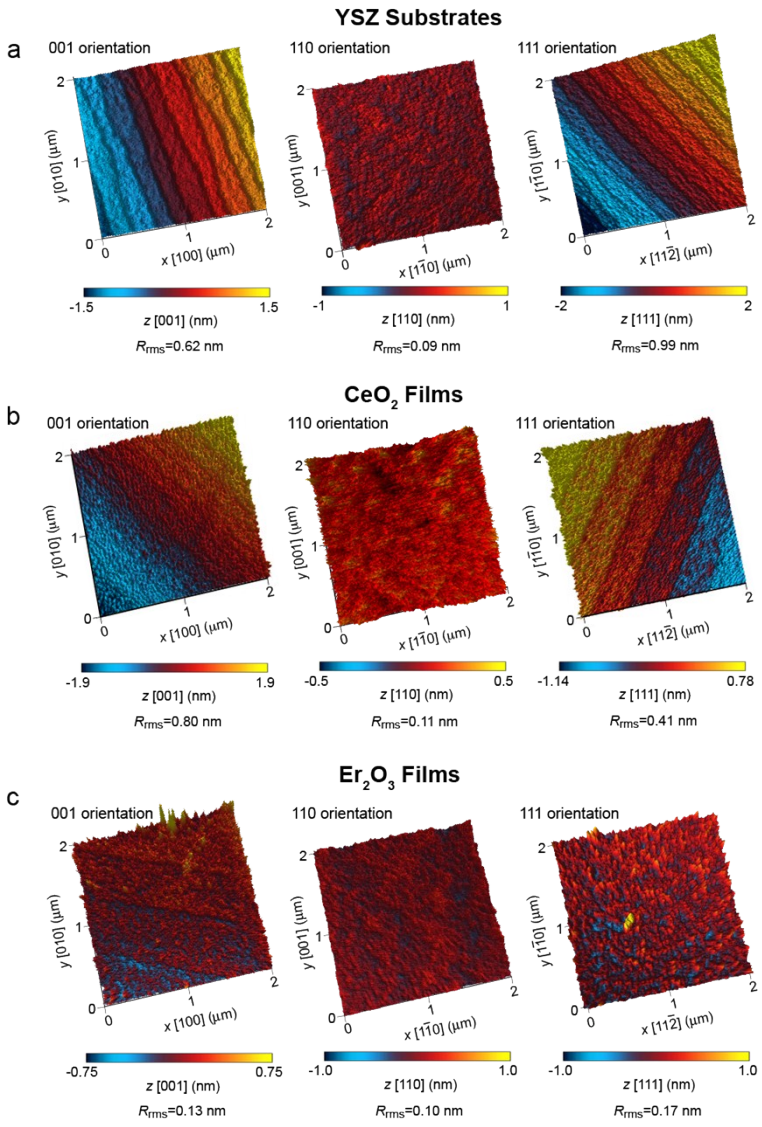

Fig. S7| AFM images of **(a)** YSZ single crystal substrates and **(b)** CeO_2 epitaxial films deposited on YSZ single crystal substrates, and **(c)** Er_2O_3 epitaxial films deposited on YSZ single crystal substrates. Low energy step and terrace structure was observed on the YSZ (001) and (111) substrates after annealing. These features were also observed after CeO_2 films were deposited on (001) and (111) YSZ substrates. The YSZ (110) substrate was featureless and the REO films deposited on (001) YSZ substrate remained featureless with a very low R_{rms}. All Er_2O_3 films were very flat with negligible roughness.

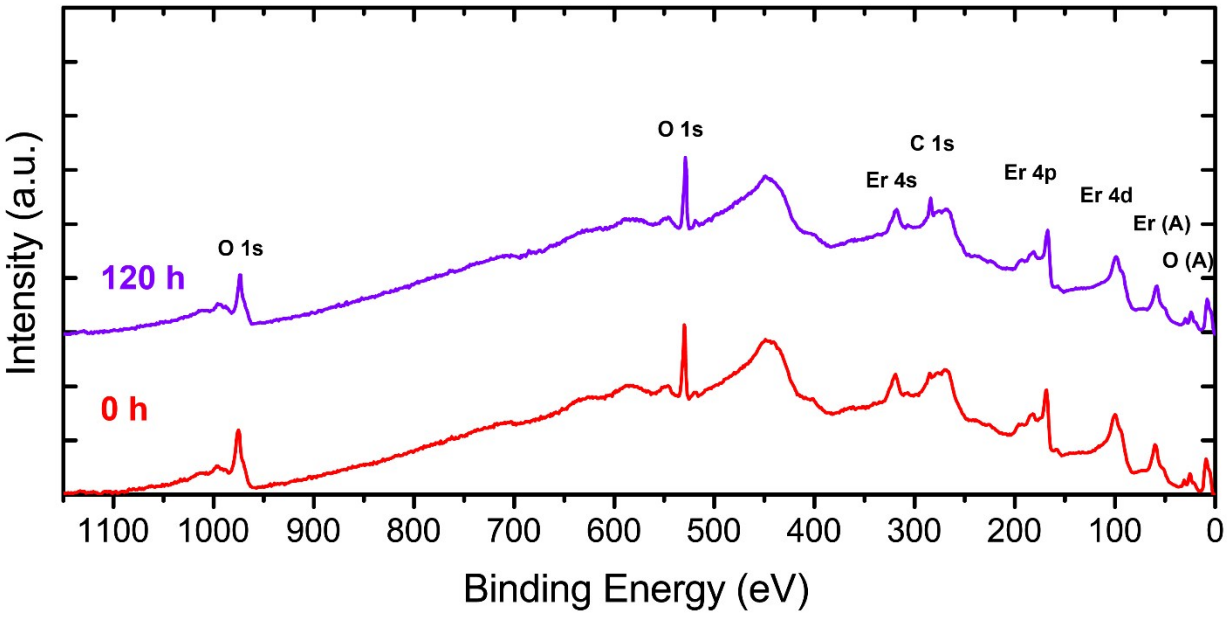

Fig. S8| X-ray photoelectron spectra of as-deposited of Er_2O_3 (001) epitaxial film on YSZ single crystal substrate and after exposure to ambient air for 120 h. Adsorption of carbon species on the specimen after storage in ambient air for 120 h is noted by the presence of the C 1s signal.

Experimental Details of X-ray Diffraction

The crystal structure, thickness, and roughness of the thin films were characterized by a four-circle high resolution X-ray diffractormeter (Rigaku ATX-G). The diffractometer is equipped with a Cu K-α source (λ = 0.154059 nm), 4 crystal monochromator and analyzer crystal. The tube voltage was set at 50 kV and a current of 300 mA was used. XRR curves were acquired by performing a 2θ-ω scan at grazing angle, 0.3° - 3.0°. Out-of-plane XRD was performed by a symmetrical 2θ-ω scan from 5° to 80°. Out-of-plane rocking curves were acquired by fixing 2θ at the position of maximum film peak and performing a ω scan, -2° to 2° relative to the selected 2θ. In-plane XRD was performed by 2θχ/φ scan. Depending on the orientation of the sample, in-plane XRD can be performed at 2 different azimuth directions. For instance, (001) and (110) oriented samples can be positioned such that [100] or [110] is parallel to the incident X-ray, hence, (200) or (110) can be detected by the $2\theta\chi/\varphi$ scan, respectively. $2\theta\chi/\varphi$ scan was performed from 5° to 80°. In-plane rocking curves were obtained by performing φ scan with 2θχ fixed at the position that give rise to maximum intensity from the thin film. Reciprocal space mapping was performed by 2θ-ω and ω scans around a diffraction spot of the REO film peak, depending on the orientation of the film and structure factor. For (001) substrate, RSM was performed around (113). For (110) substrate, the scan was performed around (240). For (111) substrate, the scan was performed around (331). For all RSM measurements, 2θχ was fixed at 0°.

Experimental Details of Scanning Transmission Electron Microscopy

Specimens for cross-sectional scanning transmission electron microscopy (STEM) analysis were prepared by conventional sample preparation techniques. First, the specimens were cut to reveal the cross section and were mounted in epoxy. Afterwards, mechanical grinding and dimple grinding were utilized to thin the specimens. Finally, the specimens were thinned to electron transparency by argon ion milling (Precision Ion Polishing System, Gatan). The STEM was operated at 200 keV to acquire high angle annular dark field (HAADF) images.

References

1 P. W. Tasker, *J. Phys. C Solid State Phys.*, 1979, **12**, 4977–4984.